Geomechanics and Engineering, *Vol. 14, No. 1 (2018) 61-69*
DOI: https://doi.org/10.12989/gae.2018.14.1.061

A new model for T-shaped combined footings part II: Mathematical model for design

Arnulfo Luévanos-Rojas*, Sandra López-Chavarria[a] and Manuel Medina-Elizondo[b]

Universidad Autónoma de Coahuila, Blvd. Revolución No, 151 Ote, CP 27000, Torreón, Coahuila, Mexico

(Received April 12, 2016, Revised May 31, 2017, Accepted June 14, 2017)

Abstract. The first part shows the optimal contact surface for T-shaped combined footings to obtain the most economical dimensioning on the soil (optimal area). This paper presents the second part of a new model for T-shaped combined footings, this part shows a the mathematical model for design of such foundations subject to axial load and moments in two directions to each column considering the soil real pressure acting on the contact surface of the footing with one or two property lines restricted, the pressure is presented in terms of an axial load, moment around the axis "X" and moment around the axis "Y" to each column, and the methodology is developed using the principle that the derived of the moment is the shear force. The classic model considers an axial load and a moment around the axis "X" (transverse axis) applied to each column, i.e., the resultant force from the applied loads is located on the axis "Y" (longitudinal axis), and its position must match with the geometric center of the footing, and when the axial load and moments in two directions are presented, the maximum pressure and uniform applied throughout the contact surface of the footing is considered the same. To illustrate the validity of the new model, a numerical example is presented to obtain the design for T-shaped combined footings subjected to an axial load and moments in two directions applied to each column. The mathematical approach suggested in this paper produces results that have a tangible accuracy for all problems.

Keywords: mathematical model for design; T-shaped combined footings; moments; bending shear; punching shear

1. Introduction

The function of a footing or a foundation is to transmit the load of the structure to the underlying soil. The choice of suitable type of footing depends on the depth at which the bearing stratum is localized, the soil condition and the type of superstructure. The foundations are classified into superficial and deep, which have important differences: in terms of geometry, the behavior of the soil, its structural functionality and its constructive systems (Bowles 2001, Das *et al*. 2006).

Superficial foundations may be of various types according to their function; isolated footing, combined footing, strip footing, or mat foundation (Bowles 2001).

The design of superficial foundations in terms of the application of loads are: 1) The footings subjected to concentric axial load, 2) The footings subjected to axial load and moment in one direction (uniaxial bending), 3) The footings subjected to axial load and moment in two directions (biaxial bending) (Bowles 2001, Das *et al*. 2006, Calabera 2000, Tomlinson 2008, McCormac and Brown 2013, González-Cuevas and Robles-Fernandez-Villegas 2005).

*Corresponding author, Ph.D.
E-mail: arnulfol_2007@hotmail.com
[a]Ph.D.
E-mail: sandylopez5@hotmail.com
[b]Ph.D.
E-mail: drmanuelmediana@yahoo.com.mx

The distribution of soil pressure under a footing is a function of the type of soil, the relative rigidity of the soil and the footing, and the depth of foundation at level of contact between footing and soil. A concrete footing on sand will have a pressure distribution similar to Fig. 1(a). When a rigid footing is resting on sandy soil, the sand near the edges of the footing tends to displace laterally when the footing is loaded. This tends to decrease in soil pressure near the edges, whereas soil away from the edges of footing is relatively confined. On the other hand, the pressure distribution under a footing on clay is similar to Fig. 1(b). As the footing is loaded, the soil under the footing deflects in a bowl-shaped depression, relieving the pressure under the middle of the footing. However, for the sake of simplicity the footing is assumed to be a perfectly rigid body, the soil is assumed to behave elastically and the distributions of stress and strain are linear in the soil just below the base of the foundation. Therefore for design purposes, it is common to assume the soil pressures are linearly distributed. The pressure distribution will be uniform if the centroid of the footing coincides with the resultant of the applied loads, as shown in Fig. 1(c) (Bowles 2001).

A combined footing is a long footing supporting two or more columns in (typically two) one row. The combined footing may be rectangular, trapezoidal or T-shaped in plan. The rectangular footing is provided when one of the projections of the footing is restricted or the width of the footing is restricted, and the column load of the property line is minor than the other. The trapezoidal footing or T-shaped is provided when the column load of the property

ISSN: 2005-307X (Print), 2092-6219 (Online)

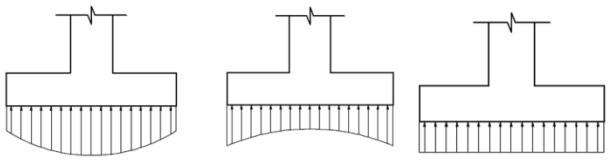

(a) (b) (c)

Fig. 1 Pressure distribution under footing, (a) footing on sand, (b) footing on clay and (c) equivalent uniform distribution

line is much more than the other. As a result, both projections of the footing beyond the faces of the columns will be restricted (Kurian 2005, Punmia *et al*. 2007, Varghese 2009).

Construction practice may dictate using only one footing for two or more columns due to:

a) Closeness of column (for example around elevator shafts and escalators).

b) Due to property line constraint, this may limit the size of footings at boundary. The eccentricity of a column placed on an edge of a footing may be compensated by tying the footing to the interior column.

Conventional method for design of combined footings by rigid method assumes that (Bowles 2001, Das *et al*. 2006, McCormac and Brown 2013, González-Cuevas and Robles-Fernandez-Villegas 2005):

1. The footing or mat is infinitely rigid, and therefore, the deflection of the footing or mat does not influence the pressure distribution.

2. The soil pressure is distributed in a straight line or a plane surface such that the centroid of the soil pressure coincides with the line of action of the resultant force of all the loads acting on foundations.

3. The minimum stress should be equal to or greater than zero, because the soil is not capable of withstand tensile stresses.

4. The maximum stress must be equal or less than the allowable capacity that can withstand the soil.

The hypothesis used in the classical model considers an axial load and a moment around the axis "X" (transverse axis) applied to each column, i.e., the resultant force from the applied loads is located on the axis "Y" (longitudinal axis), and its position must match with the geometric center of the footing, and when the axial load and moments in two directions are presented, the maximum pressure and uniform applied throughout the contact surface of the footing is considered the same. Then the equation of the biaxial bending is used to obtain the stresses acting on the contact surface of the combined footings, which must meet the following conditions: 1) The minimum stress should be equal to or greater than zero, because the soil is not capable of withstand tensile stresses, 2) The maximum stress must be equal or less than the allowable capacity that can withstand the soil (Das *et al.* 2006, Bowles 2001, Calabera-Ruiz 2000, Tomlinson 2008).

Guler and Celep (2005) presented the response of a rectangular plate-column system on a tensionless winkler foundation subjected to static and dynamic loads.

Chen *et al.* (2011) proposed the nonlinear partial differential equations of motion for a hybrid composite plate subjected to initial stresses on elastic foundations are established to investigate its nonlinear vibration behavior.

Smith-Pardo (2011) in this study presents a performance-based framework for soil-structure systems using simplified rocking foundation models.

Shahin and Cheung (2011) presented the stochastic design charts for bearing capacity of strip footings.

Zhang *et al.* (2011) presented a nonlinear analysis of finite beam resting on winkler with consideration of beam-soil interface resistance effect.

Agrawal and Hora (2012) proposed the building frame and its foundation along with the soil on which it rests, together constitute a complete structural system.

Rad (2012) realized the study on the static behavior of bi-directional functionally graded (FG) non-uniform thickness circular plate resting on quadratically gradient elastic foundations (Winkler-Pasternak type) subjected to axisymmetric transverse and in-plane shear loads is carried out by using state-space and differential quadrature methods.

Maheshwari and Khatri (2012) estimated the influence of inclusion of geosynthetic layer on response of combined footings on stone column reinforced earth beds.

Orbanich *et al.* (2012) showed a study on strenghtening and repair of concrete foundation beams whit fiber composite materials.

Mohamed *et al*. (2013) presented the generalized Schmertmann equation for settlement estimation of shallow footings in saturated and unsaturated sands.

Luévanos-Rojas *et al.* (2013) proposed a design of isolated footings of rectangular form using a new model.

Orbanich and Ortega (2013) this study aimed to investigate the mechanical behavior of rectangular foundation plates with perimetric beams and internal stiffening beams of the plate is herein analyzed, taking the foundation design into account.

Dixit and Patil (2013) showed an experimental estimate of Nγ values and corresponding settlements for square footings on finite layer of sand.

ErzÍn and Gul (2013) presented the use of neural networks for the prediction of the settlement of pad footings on cohesionless soils based on standard penetration test.

Cure *et al*. (2014) proposed the decrease trends of ultimate loads of eccentrically loaded model strip footings close to a slope.

Luévanos-Rojas (2014a) presented a design of isolated footings of circular form using a new model.

Luévanos-Rojas (2014b) proposed a design of boundary combined footings of rectangular shape using a new model.

Uncuoğlu (2015) showed a study on bearing capacity of square footings on sand layer overlying clay.

Luévanos-Rojas (2015) presented a design of boundary combined footings of trapezoidal form using a new model.

Luévanos-Rojas (2016a) made a comparative study for the design of rectangular and circular isolated footings using new models.

Luévanos-Rojas (2016b) presented a new model for the design of boundary combined rectangular footings with two opposing restricted sides.

This paper presents the second part of a new model for

T-shaped combined footings, this part shows a the mathematical model for design of such foundations subject to axial load and moments in two directions to each column considering the soil real pressure acting on the contact surface of the footing with one or two property lines restricted, the pressure is presented in terms of an axial load, moment around the axis "X" and moment around the axis "Y" to each column, and the methodology is developed using the principle that the derived of the moment is the shear force. The first part shows the optimal contact surface for T-shaped combined footings to obtain the most economical dimensioning on the soil (optimal area). To illustrate the validity of the new model, a numerical example is presented to obtain the design for T-shaped combined footings subjected to an axial load and moments in two directions applied to each column.

2. Methodology

2.1 General conditions

According to Building Code Requirements for Structural Concrete (ACI 318-13) and Commentary the critical sections are: 1) the maximum moment is located in face of column, pedestal, or wall, for footings supporting a concrete column, pedestal, or wall; 2) bending shear is presented at a distance "*d*" (distance from extreme compression fiber to centroid of longitudinal tension reinforcement) shall be measured from face of column, pedestal, or wall for footings supporting a column, pedestal, or wall; 3) punching shear is localized so that it perimeter "b_o" is a minimum but need not approach closer than "*d/2*" to: (a) Edges or corners of columns, concentrated loads, or reaction areas; and (b) Changes in slab thickness such as edges of capitals, drop panels, or shear caps.

The general equation for any type of footings subjected to bidirectional bending (Luévanos-Rojas *et al.* 2013, Luévanos-Rojas 2014a, b, 2015, 2016a, b, Gere and Goodno 2009)

$$\sigma = \frac{P}{A} \pm \frac{M_x y}{I_x} \pm \frac{M_y x}{I_y} \tag{1}$$

where σ is the stress exerted by the soil on the footing (soil pressure), A is the contact area of the footing, P is the axial load applied at the center of gravity of the footing, M_x is the moment around the axis "X", M_y is the moment around the axis "Y", x is the distance in the direction "X" measured from the axis "Y" to the fiber under study, y is the distance in direction "Y" measured from the axis "X" to the farthest under study, I_y is the moment of inertia around the axis "Y" and I_x is the moment of inertia around the axis "X".

2.2 New model for design of the T-shaped combined footings

Fig. 3 of the Part 1 shows a T-shaped combined footing under axial load and moment in two directions (biaxial bending) in each column, the pressure below the footing vary linearly (Luévanos-Rojas *et al.* 2013, Luévanos-Rojas 2014a, b, 2015, 2016a, b).

Fig. 4 of the Part 1 presents the diagram of pressure below the T-shaped combined footing and also the stresses in each vertex.

The stresses anywhere of the contact surface the structural member due to the pressure that is exerted by the soil for the T-shaped combined footing are obtained:

The stress in the main direction (axis "*Y*") is

$$\sigma(x,y) = \frac{R}{A} + \frac{M_{xT} y}{I_x} + \frac{M_{yT} x}{I_y} \tag{2}$$

where R, M_{xT}, M_{yT}, A, I_x and I_y of part 1 are

$$R = P_1 + P_2 \tag{3}$$

$$M_{xT} = \frac{R[(a-b_2){b_1}^2 + b^2 b_2]}{2[(a-b_2)b_1 + b b_2]} + M_{x1} + M_{x2} - \frac{R c_2}{2} - P_2 L \tag{4}$$

$$M_{yT} = M_{y1} + M_{y2} \tag{5}$$

$$A = (a-b_2)b_1 + b b_2 \tag{6}$$

$$I_x = \frac{a^2 {b_1}^4 + 2a b_1 b_2 (b-b_1)\left(2b^2 - b b_1 + {b_1}^2\right) + {b_2}^2 (b-b_1)^4}{12[(a-b_2)b_1 + b b_2]} \tag{7}$$

$$I_y = \frac{b_1 a^3 + (b-b_1){b_2}^3}{12} \tag{8}$$

The stresses in the transverse direction to the main direction (axis "*X*") are:

To the number column 1 is

$$\sigma_{P_1}(x,y) = \frac{P_1}{{w_1}^3 a} + \frac{12[M_{x1} + P_1(w_1 - c_2)/2]y}{{w_1}^3 a} + \frac{12 M_{y1} x}{w_1 a^3} \tag{9}$$

To the number column 2 is

$$\sigma_{P_2}(x,y) = \frac{P_2}{{w_2}^3 b_2} + \frac{12[M_{x2} - P_2(w_2 - c_4 - 2v)/2]y}{{w_2}^3 b_2} + \frac{12 M_{y2} x}{w_2 {b_2}^3} \tag{10}$$

where w_1 and w_2 are the widths of the analysis surface for the columns 1 and 2 in the transverse direction to the main direction, these are $w_1=c_2+d/2$, $w_2=c_4+d/2+v$. If $d/2 \leq v \rightarrow v=d/2$, and if $d/2 \geq v \rightarrow v=b-L-(c_2+c_4)/2$.

Geometry conditions are

$$b \geq \frac{c_2}{2} + L + \frac{c_4}{2} \tag{11}$$

$$b = y_s + y_i \tag{12}$$

$$y_s = \frac{(a-b_2){b_1}^2 + b^2 b_2}{2[(a-b_2)b_1 + b b_2]} \tag{13}$$

$$y_i = \frac{(2b-b_1)(a-b_2)b_1 + b^2 b_2}{2[(a-b_2)b_1 + b b_2]} \tag{14}$$

2.2.1 Moments

Critical sections for moments are presented in section *a'-a'*, *b'-b'*, *c'-c'*, *d'-d'*, *e'-e'*, *f'-f'* and *g'-g'*, as shown in Fig. 2.

2.2.1.1 Moment around the axis y_1'- y_1' of $0 \leq x_1 \leq a/2$

Shear force "V_{x1}" is found through the volume of pressure the area formed by the axis y_1'-y_1' with a width "$w_1=c_2+d/2$" and the free end (left side of the Fig. 2) of the footing

$$V_{x_1} = -\int_{-w_1/2}^{w_1/2}\int_{x_1}^{a/2}\sigma_{P_1}(x,y)dxdy = \frac{6M_{y1}{x_1}^2}{a^3} + \frac{P_1x_1}{a} - \frac{P_1a+3M_{y1}}{2a} \quad (15)$$

If the derived of the moment is the shear force, therefore, it is presented as follows

$$V_{x_1} = \frac{dM_{y_1}{}'}{dx_1} \quad (16)$$

where $M_{y1}{}'$ is the moment around the axis "y_1'" and V_{x1} is the shear force at a distance "x_1".

Then, the moment is obtained as follows

$$M_{y_1}{}' = \int\left(\frac{6M_{y1}{x_1}^2}{a^3} + \frac{P_1x_1}{a} - \frac{P_1a+3M_{y1}}{2a}\right)dx_1 = \frac{2M_{y1}{x_1}^3}{a^3} + \frac{P_1{x_1}^2}{2a} - \frac{P_1x_1}{2} - \frac{3M_{y1}x_1}{2a} + C_1 \quad (17)$$

Substituting "$x_1 = a/2$" and $M_{y1}{}' = 0$ into Eq. (17), the constant "C_1" is obtained

$$C_1 = \frac{P_1a}{8} + \frac{M_{y1}}{2} \quad (18)$$

Now, substituting Eq. (18) into Eq. (17) to obtain the moments equation, this is

$$M_{y_1}{}' = \frac{P_1(2x_1-a)^2}{8a} + \frac{M_{y1}(4{x_1}^3 - 3a^2x_1 + a^3)}{2a^3} \quad (19)$$

Substituting "$x_1=c_1/2$" into Eq. (19) to obtain $M_{a'}$, this is

$$M_{a'} = \frac{[P_1a^2 + 2M_{y1}(2a+c_1)](a-c_1)^2}{8a^3} \quad (20)$$

2.2.1.2 Moment around the axis y_2'-y_2' of $0 \le x_2 \le b_2/2$

Shear force "V_{x2}" is found through the volume of pressure the area formed by the axis y_2'-y_2' with a width "$w_2=c_2+d$" and the free end (left side of the Fig. 2) of the footing

$$V_{x_2} = -\int_{-w_2/2}^{w_2/2}\int_{x_2}^{b_2/2}\sigma_{P_2}(x,y)dxdy = \frac{6M_{y2}{x_2}^2}{{b_2}^3} + \frac{P_2x_2}{b_2} - \frac{P_2b_2+3M_{y2}}{2b_2} \quad (21)$$

Taking into account that the derived of the moment is the shear force is presented as follows

$$V_{x_2} = \frac{dM_{y_2}{}'}{dx_2} \quad (22)$$

where $M_{y2}{}'$ is the moment around the axis "y_2'" and V_{x2} is the shear force at a distance "x_2".

Therefore, the moment is presented

$$M_{y_2}{}' = \int\left(\frac{6M_{y2}{x_2}^2}{{b_2}^3} + \frac{P_2x_2}{b_2} - \frac{P_2b_2+3M_{y2}}{2b_2}\right)dx_2 = \frac{2M_{y2}{x_2}^3}{{b_2}^3} + \frac{P_2{x_2}^2}{2b_2} - \frac{P_2x_2}{2} - \frac{3M_{y2}x_2}{2b_2} + C_2 \quad (23)$$

Substituting "$x_2 = b_2/2$" and $M_{y2}{}' = 0$ into Eq. (23), the constant "C_2" is obtained

$$C_2 = \frac{P_2b_2}{8} + \frac{M_{y2}}{2} \quad (24)$$

Now, substituting Eq. (24) into Eq. (23) to obtain the moments equation, this is

$$M_{y_2}{}' = \frac{P_2(2x_2-b_2)^2}{8b_2} + \frac{M_{y2}(4{x_2}^3 - 3{b_2}^2x_2 + {b_2}^3)}{2{b_2}^3} \quad (25)$$

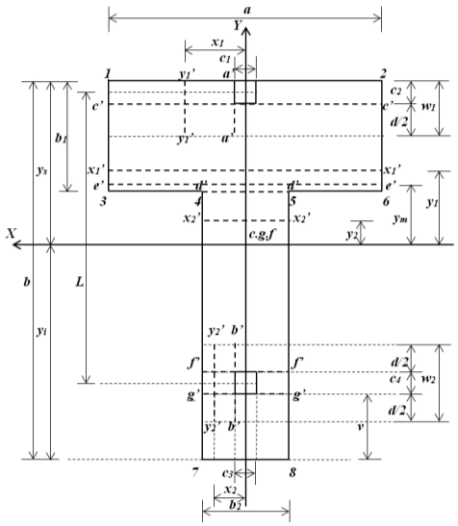

Fig. 2 Critical sections for moments

Substituting "$x_2 = c_3/2$" into Eq. (25) to obtain $M_{b'}$, this is

$$M_{b'} = \frac{[P_2{b_2}^2 + 2M_{y2}(2b_2+c_3)](b_2-c_3)^2}{8{b_2}^3} \quad (26)$$

2.2.1.3 Moment around the axis x_1'-x_1' of y_s–$c_2/2 \le y_1 \le y_s$

The shear force "V_{y1}" is found through the volume of pressure the area formed by the axis x_1'-x_1' with a width "a" and the free end (top side of the Fig. 2) of the footing

$$V_{y_1} = -\int_{y_1}^{y_s}\int_{-a/2}^{a/2}\sigma(x,y)dxdy = \frac{M_{xT}a{y_1}^2}{2I_x} + \frac{Ray_1}{A} - \frac{2RI_xay_s + M_{xT}Aay_s^2}{2AI_x} \quad (27)$$

Considering that the derived of the moment is the shear force is obtained

$$V_{y_1} = \frac{dM_{x_1}{}'}{dy_1} \quad (28)$$

where $M_{x1}{}'$ is the moment around the axis "x_1'" and V_{y1} is the shear force at a distance "y_1".

Therefore, the moment is presented

$$M_{x_1}{}' = \int\left(\frac{M_{xT}a{y_1}^2}{2I_x} + \frac{Ray_1}{A} - \frac{2RI_xay_s + M_{xT}Aay_s^2}{2AI_x}\right)dy_1 = \frac{M_{xT}a{y_1}^3}{6I_x} + \frac{Ray_1^2}{2A} - \frac{Rayy_1}{A} - \frac{M_{xT}ay_s^2y_1}{2I_x} + C_3 \quad (29)$$

Substituting "$y_1=y_s$" and $M_{x1}=0$ into Eq. (29), the constant "C_3" is found

$$C_3 = \frac{Ray_s^2}{2A} + \frac{M_{xT}ay_s^3}{3I_x} \quad (30)$$

Now, substituting Eq. (30) into Eq. (29) to obtain the moments equation, this is

$$M_{x_1} = \frac{Ra(y_1-y_s)^2}{2A} + \frac{M_{xT}a({y_1}^3 - 3y_s^2y_1 + 2y_s^3)}{6I_x} \quad (31)$$

Substituting "$y_1=y_s-c_2/2$" into Eq. (31) to obtain $M_{c2/2}$ (Moment in the column center 1), this is

$$M_{c_2/2'} = \frac{[6RI_x + M_{xT}A(6y_s-c_2)]ac_2^2}{48AI_x} \quad (32)$$

2.2.1.4 Moment around the axis x_1'-x_1' of y_s–b_1≤y_1≤y_s–c_2/2

Shear force "V_{y1}" is found through the volume of pressure the area formed by the axis x_1'-x_1' with a width "a" and the free end (top side of the Fig. 2) of the footing

$$V_{y_1} = P_1 - \int_{y_1}^{y_s}\int_{-a/2}^{a/2}\sigma(x,y)dxdy = P_1 + \frac{M_{xT}ay_1^{\,2}}{2I_x} + \frac{Ray_1}{A} - \frac{2RI_xay_s + M_{xT}Aay_s^{\,2}}{2AI_x} \quad (33)$$

The moment by Eq. (28) is presented

$$\begin{aligned} M_{x_1'} &= \int\left(P_1 + \frac{M_{xT}ay_1^{\,2}}{2I_x} + \frac{Ray_1}{A} - \frac{2RI_xay_s + M_{xT}Aay_s^{\,2}}{2AI_x}\right)dy_1 \\ &= P_1y_1 + \frac{M_{xT}ay_1^{\,3}}{6I_x} + \frac{Ray_1^{\,2}}{2A} - \frac{Ray_sy_1}{A} - \frac{M_{xT}ay_s^{\,2}y_1}{2I_x} + C_4 \end{aligned} \quad (34)$$

Substituting "y_1=y_s–c_2/2" and $M_{c2/2'}$={[6RI_x+$M_{xt}A$(6$_{ys}$–c_2)]}/48AI_x–M_{x1} into Eq. (34), the constant "C_4" is obtained

$$C_4 = \frac{ay_s^{\,2}(3RI_x + 2M_{xT}Ay_s) - 3P_1AI_x(2y_s - c_2)}{6AI_x} - M_{x1} \quad (35)$$

Now, substituting Eq. (35) into Eq. (34) to obtain the moments equation, this is

$$M_{x_1'} = \frac{P_1(2y_1 - 2y_s + c_2)}{2} + \frac{Ra(y_1 - y_s)^2}{2A} + \frac{M_{xT}a(y_1^{\,3} - 3y_s^{\,2}y_1 + 2y_s^{\,3})}{6I_x} - M_{x1} \quad (36)$$

Substituting "y_1=y_s–c_2" into Eq. (36) to obtain $M_{c'}$, this is

$$M_{c'} = \frac{c_2\{ac_2[3RI_x + M_{xT}A(3y_s - c_2)] - 3P_1AI_x\}}{6AI_x} - M_{x1} \quad (37)$$

Substituting "y_1=y_s–b_1" " into Eq. (36) to obtain $M_{d'}$, this is

$$M_{d'} = \frac{ab_1^{\,2}[3RI_x + M_{xT}A(3y_s - b_1)] - 3P_1AI_x(2b_1 - c_2)}{6AI_x} - M_{x1} \quad (38)$$

If there is a maximum moment in the interval "y_s–b_1≤y_1=y_m≤y_s–c_2/2" (When the shear force is zero, the moment should be the maximum). Therefore, Eq. (33) is used to obtain the position the axis e'-e', where the maximum moment is located.

The position of the axis *e'-e'* is obtained

$$y_m = \frac{-RI_xa \pm \sqrt{a^2(RI_x + M_{xT}Ay_s)^2 - 2P_1M_{xT}A^2I_xa}}{M_{xT}Aa} \quad (39)$$

Now, if y_1=y_m and substituting Eq. (39) into Eq. (36) to obtain $M_{e'}$ (maximum moment).

2.2.1.5 Moment around the axis x_2'-x_2' of y_s–(L+c_2/2)≤y_2 ≤y_s–b_1

Shear force "V_{y2}" is found through the volume of pressure the area formed by the axis x_2'-x_2' with a width "b_2" and the free end (top side of the Fig. 2) of the footing

$$\begin{aligned} V_{y_2} &= P_1 - \int_{y_s-b_1}^{y_s}\int_{-a/2}^{a/2}\sigma(x,y)dxdy - \int_{y_2}^{y_s-b_1}\int_{-b_2/2}^{b_2/2}\sigma(x,y)dxdy \\ &= P_1 + \frac{M_{xT}b_2y_2^{\,2}}{2I_x} + \frac{Rb_2y_2}{A} \\ &\quad - \frac{2RI_x[ab_1 + b_2(y_s - b_1)] + M_{xT}A[ay_s^{\,2} - (a - b_2)(y_s - b_1)^2]}{2AI_x} \end{aligned} \quad (40)$$

The moment by Eq. (28) is obtained

$$\begin{aligned} M_{x_2'} &= \int\left(P_1 + \frac{M_{xT}b_2y_2^{\,2}}{2I_x} + \frac{Rb_2y_2}{A} \right. \\ &\quad \left. - \frac{2RI_x[ab_1 + b_2(y_s - b_1)] + M_{xT}A[ay_s^{\,2} - (a - b_2)(y_s - b_1)^2]}{2AI_x}\right)dy_2 \\ &= P_1y_2 + \frac{M_{xT}b_2y_2^{\,3}}{6I_x} + \frac{Rb_2y_2^{\,2}}{2A} \\ &\quad - \frac{\{2RI_x[ab_1 + b_2(y_s - b_1)] + M_{xT}A[ay_s^{\,2} - (a - b_2)(y_s - b_1)^2]\}y_2}{2AI_x} + C_5 \end{aligned} \quad (41)$$

Substituting "y_2=y_s–b_1" and $M_{d'} = \{ab_1^{\,2}[3RI_x + M_{xT}A(3y_s - b_1)] - 3P_1AI_x(2b_1 - c_2)\}/6AI_x - M_{x1}$ into Eq. (41), the constant "C_5" is obtained

$$C_5 = \frac{R[ay_s^{\,2} + (b_2 - a)(y_s - b_1)^2]}{2A} + \frac{M_{xT}[2ay_s^{\,3} - 2(a - b_2)(y_s - b_1)^3]}{6I_x} - \frac{P_1(2y_s - c_2)}{2} - M_{x1} \quad (42)$$

Now, substituting Eq. (42) into Eq. (41) to obtain the moments equation, this is

$$\begin{aligned} M_{x_2'} &= \frac{P_1(2y_2 - 2y_s + c_2)}{2} + \frac{R[ab_1(2y_s - 2y_2 - b_1) + b_2(y_2 - y_s + b_1)^2]}{2A} \\ &\quad + \frac{M_{xT}\{ay_s^{\,2}(2y_s - 3y_2) + b_2y_2^{\,3} - (a - b_2)(y_s - b_1)^2(2y_s - 2b_1 - 3y_2)\}}{6I_x} \\ &\quad - M_{x1} \end{aligned} \quad (43)$$

Substituting "y_2=y_s–(L+c_2/2–c_4/2)" into Eq. (43) to obtain $M_{f'}$, this is shown as follows

$$\begin{aligned} M_{f'} &= \frac{R[b_2(L + c_2/2 - c_4/2 - b_1)^2 + ab_1(2L - b_1 + c_2 - c_4)]}{2A} \\ &\quad + \frac{M_{xT}b_1(a - b_2)\left[4b_1^{\,2} - 3b_1(2y_s + c_2 + 2L - c_4) + 6y_s(c_2 + 2L - c_4)\right]}{12I_x} \\ &\quad + \frac{M_{xT}b_2(c_2 + 2L - c_4)^2(6y_s - c_2 - 2L + c_4)}{48I_x} - \frac{P_1(2L - c_4)}{2} - M_{x1} \end{aligned} \quad (44)$$

Substituting "y_2 y_s–(L + c_2/2)" into Eq. (43) to obtain to obtain $M_{c4/2'}$ (Moment in the column center 2), this is

$$\begin{aligned} M_{c_4/2'} &= \frac{R[b_2(L + c_2/2 - b_1)^2 + ab_1(2L - b_1 + c_2)]}{2A} \\ &\quad + \frac{M_{xT}b_1(a - b_2)\left[4b_1^{\,2} - 3b_1(2y_s + c_2 + 2L) + 6y_s(c_2 + 2L)\right]}{12I_x} \\ &\quad + \frac{M_{xT}b_2(c_2 + 2L)^2(6y_s - c_2 - 2L)}{48I_x} - P_1L - M_{x1} \end{aligned} \quad (45)$$

If there is a maximum moment in the interval "y_s–(L+c_2/2)≤y_2=y_m≤y_s–b_1" (When the shear force is zero, the moment should be the maximum). Therefore, Eq. (40) is used to obtain the position the axis *e'-e'*, where the maximum moment is located.

The position the axis *e'-e'* is obtained

$$\begin{aligned} y_m &= \\ &\frac{-RI_xb_2 \pm \sqrt{b_2^{\,2}[RI_x + M_{xT}A(y_s - b_1)]^2 + M_{xT}Ab_2\{ab_1[2RI_x + M_{xT}A(2y_s - b_1)] - 2P_1AI_x\}}}{M_{xT}Ab_2} \end{aligned} \quad (46)$$

Now, if y_2=y_m and substituting Eq. (46) into Eq. (43) to obtain the maximum moment.

2.2.1.6 Moment around the axis x_2'-x_2' of y_s–b≤y_2≤y_s–(L+c_2/2)

Shear force "V_{y2}" is found through the volume of pressure the area formed by the axis x_2'-x_2' with a width "b_2" and the free end (top side of the Fig. 2) of the footing

$$\begin{aligned} V_{y_2} &= P_1 + P_2 - \int_{y_s-b_1}^{y_s}\int_{-a/2}^{a/2}\sigma(x,y)dxdy - \int_{y_2}^{y_s-b_1}\int_{-b_2/2}^{b_2/2}\sigma(x,y)dxdy \\ &= P_1 + P_2 + \frac{M_{xT}b_2y_2^{\,2}}{2I_x} + \frac{Rb_2y_2}{A} \\ &\quad - \frac{2RI_x[ab_1 + b_2(y_s - b_1)] + M_{xT}A[ay_s^{\,2} - (a - b_2)(y_s - b_1)^2]}{2AI_x} \end{aligned} \quad (47)$$

The moment by Eq. (28) is obtained

$$\begin{aligned} M_{x_2'} &= \int\left(P_1 + P_2 + \frac{M_{xT}b_2y_2^{\,2}}{2I_x} + \frac{Rb_2y_2}{A} \right. \\ &\quad \left. - \frac{2RI_x[ab_1 + b_2(y_s - b_1)] + M_{xT}A[ay_s^{\,2} - (a - b_2)(y_s - b_1)^2]}{2AI_x}\right)dy_2 \\ &= (P_1 + P_2)y_2 + \frac{M_{xT}b_2y_2^{\,3}}{6I_x} + \frac{Rb_2y_2^{\,2}}{2A} \\ &\quad - \frac{\{2RI_x[ab_1 + b_2(y_s - b_1)] + M_{xT}A[ay_s^{\,2} - (a - b_2)(y_s - b_1)^2]\}y_2}{2AI_x} + C_6 \end{aligned} \quad (48)$$

Substituting "y_2=y_s–(L+c_2/2)" and $M_{c_4/2'} = R[b_2(L + c_2/2 - b_1)^2 + ab_1(2L - b_1 + c_2)]/2A + M_{xT}\{(a - b_2)\left[16b_1^{\,3} - 12b_1^{\,2}(2y_s + c_2 + 2L) + 24b_1y_s(c_2 + 2L)\right] + b_2(c_2 + 2L)^2(6y_s - c_2 - 2L)\}/6I_x - M_{x1} - M_{x2} - P_1L$ into Eq. (48) to find, the constant "C_6" is obtained

$$C_6=\frac{R[ab_1(2y_s-b_1)+b_2(y_s-b_1)^2]}{2A}+\frac{M_{xT}[ay_s{}^3-(a-b_2)(y_s-b_1)^3]}{3I_x}-M_{x1}-M_{x2}-P_1L-R[y_s-(L+c_2/2)] \quad (49)$$

Now, substituting Eq. (49) into Eq. (48) to obtain the moments equation, this is

$$M_{x_2'}=Ry_2+\frac{M_{xT}b_2y_2{}^3}{6I_x}+\frac{Rb_2y_2{}^2}{2A}-\frac{R[ab_1+b_2(y_s-b_1)]y_2}{A}-\frac{M_{xT}[ay_s{}^2-(a-b_2)(y_s-b_1)^2]y_2}{2I_x}+\frac{R[ab_1(2y_s-b_1)+b_2(y_s-b_1)^2]}{2A}+\frac{M_{xT}[ay_s{}^3-(a-b_2)(y_s-b_1)^3]}{3I_x}-M_{x1}-M_{x2}-P_1L-R\left[y_s-\left(L+\frac{c_2}{2}\right)\right] \quad (50)$$

Substituting "$y_2=y_s-(L+c_2/2+c_4/2)$" into Eq. (50) to obtain to obtain $M_{g'}$, this is

$$M_{g'}=\frac{R[b_2(L+c_2/2+c_4/2-b_1)^2+ab_1(2L-b_1+c_2+c_4)]}{2A}+\frac{M_{xT}b_1(a-b_2)[4b_1{}^2-3b_1(2y_s+c_2+2L+c_4)+6y_s(c_2+2L+c_4)]}{12I_x}+\frac{M_{xT}b_2(c_2+2L+c_4)^2(6y_s-c_2-2L-c_4)}{48I_x}-\frac{P_1(2L+c_4)}{2}-\frac{P_2c_4}{2}-M_{x1}-M_{x2} \quad (51)$$

2.2.2 Bending shear (unidirectional shear force)

Critical sections for bending shear are obtained at a distance *"d"* starting the junction of the column with the footing as seen in Fig. 3, these are presented in sections *h'-h', i'-i", j'-j', k'-k', l'-l'* and *m'-m'*.

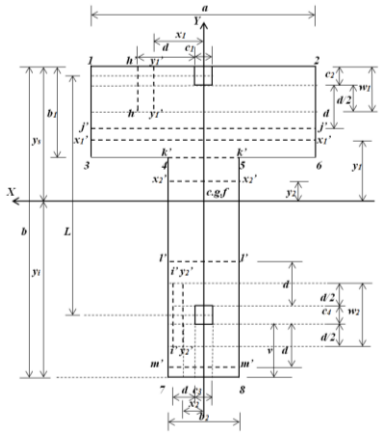

Fig. 3 Critical sections for bending shear

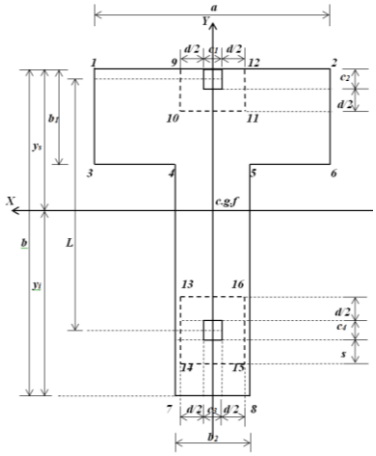

Fig. 4 Critical sections for the punching shear supporting a rectangular column

2.2.2.1 Bending shear on axis h'-h'

Substituting "$x_1=c_1/2+d$" into Eq. (15) to obtain the bending shear on the axis *h'-h'* of the footing *"$V_{fh'}$"*, this is

$$V_{fh'}=-\frac{[P_1a^2+3M_{y1}(a+c_1+2d)](a-c_1-2d)}{2a^3} \quad (52)$$

2.2.2.2 Bending shear on axis i'-i'

Substituting "$x_2=c_3/2+d$" into Eq. (21) to obtain the bending shear on the axis *i'-i'* of the footing *"$V_{fi'}$"*, this is

$$V_{fi'}=-\frac{[P_2b_2{}^2+3M_{y2}(b_2+c_3+2d)](b_2-c_3-2d)}{2b_2{}^3} \quad (53)$$

2.2.2.3 Bending shear on axis j'-j' (If $y_1 \geq y_s - b_1$)

Substituting "$y_1=y_s-c_2-d$" into Eq. (33) to obtain the bending shear on the axis *j'-j'* of the footing *"$V_{fj'}$"*, this is

$$V_{fj'}=P_1-\frac{[2RI_x+M_{xT}A(2y_s-c_2-d)]a(c_2+d)}{2AI_x} \quad (54)$$

2.3.2.4 Bending shear on axis k'-k'

Substituting "$y_1=y_s-b_1$" into Eq. (33) to obtain the bending shear on the axis *k'-k'* of the footing *"$V_{fk'}$"*, this is

$$V_{fk'}=P_1-\frac{[2RI_x+M_{xT}A(2y_s-b_1)]ab_1}{2AI_x} \quad (55)$$

2.2.2.5 Bending shear on axis j'-j' (If $y_2 \leq y_s - b_1$)

Substituting "$y_2=y_s-c_2-d$" into Eq. (40) to obtain the bending shear on the axis *j'-j'* of the footing "$V_{fj'}$", this is

$$V_{fj'}=P_1+\frac{R[b_2(b_1-c_2-d)-ab_1]}{A}+\frac{M_{xT}[b_2(y_s-c_2-d)^2-ay_s{}^2+(a-b_2)(y_s-b_1)^2]}{2I_x} \quad (56)$$

2.2.2.6 Bending shear on axis l'-l'

Substituting "$y_2=y_s-c_2/2-L+c_4/2+d$" into Eq. (40) to obtain the bending shear on the axis *l'-l'* of the footing *"$V_{fl'}$"*, this is

$$V_{fl'}=P_1+\frac{R[b_2(b_1-c_2/2-L+c_4/2+d)-ab_1]}{A}+\frac{M_{xT}[b_2(y_s-c_2/2-L+c_4/2+d)^2-ay_s{}^2+(a-b_2)(y_s-b_1)^2]}{2I_x} \quad (57)$$

2.2.2.7. Bending shear on axis m'-m'

Substituting "$y_2=y_s-c_2/2-L-c_4/2-d$" into Eq. (47) to obtain the bending shear on the axis *m'-m'* of the footing "$V_{fm'}$", this is

$$V_{fm'}=P_1+P_2+\frac{R[b_2(b_1-c_2/2-L-c_4/2-v)-ab_1]}{A}+\frac{M_{xT}[b_2(y_s-c_2/2-L-c_4/2-v)^2-ay_s{}^2+(a-b_2)(y_s-b_1)^2]}{2I_x} \quad (58)$$

where "v" must meet the following relationships: if $d \leq v \rightarrow v=d$, and if $d \geq v \rightarrow v=0$, because the critical side is found outside the footing.

2.2.3 Punching shear (bidirectional shear force)

Critical section for the punching shear appears at a distance *"$d/2$"* starting the junction of the column with the footing in the two directions, as shown in Fig. 4.

2.2.3.1 Punching shear for column 1

Critical section for the punching shear is presented in rectangular section formed by points 9, 10, 11 and 12. Punching shear acting on the footing "V_{p1}" is the force "P_1" acting on column 1 subtracting the pressure volume of the area formed by the points 9, 10, 11 and 12

$$V_{p1} = P_1 - \int_{y_s-(c_2+d/2)}^{y_s} \int_{-(c_1+d)/2}^{(c_1+d)/2} \sigma(x,y)dxdy = P_1 - \frac{[2RI_x + M_{xT}A(2y_s - c_2 - d/2)](c_1 + d)(c_2 + d/2)}{2AI_x} \quad (59)$$

2.2.3.2 Punching shear for column 2

The critical section for the punching shear is presented in rectangular section formed by points 13, 14, 15 and 16. Punching shear acting on the footing "V_{p2}" is the force "P_2" acting on column 2 subtracting the pressure volume of the area formed by the points 13, 14, 15 and 16

$$V_{p2} = P_2 - \int_{y_s-[L+s+(c_2+c_4)/2]}^{y_s-[L+(c_2-c_4-d)/2]} \int_{-(b_2-c_3-d)/2}^{(b_2-c_3-d)/2} \sigma(x,y)dxdy = P_2 - \frac{\{4RI_x + M_{xT}A[2(2y_s - 2L - s) - 2c_2 + d]\}(b_2 - c_3 - d)(2c_4 + d + 2s)}{8AI_x} \quad (60)$$

where "s" must meet the following relationships: if $d/2 \leq b-L-(c_2+c_4)/2 \rightarrow s=d/2$, and if $d/2 \geq b-L-(c_2+c_4)/2 \rightarrow s=b-L-(c_2+c_4)/2$.

3. Numerical example

The design of a T-shaped combined footing supporting two square columns is presented in Fig. 2, with the information following: the two columns are of 40x40 cm; L=6.00 m; H=2.0 m; P_{D1}=600 *kN*; P_{L1}=400 *kN*; M_{Dx1}=160 *kN-m*; M_{Lx1}=140 *kN-m*; M_{Dy1}=120 *kN-m*; M_{Ly1}=80 *kN-m*; P_{D2}=300 *kN*; P_{L2}=200 *kN*; M_{Dx2}=80 *kN*-m; M_{Lx2}=70 *kN-m*; M_{Dy2}=120 *kN-m*; M_{Ly2}=80 *kN-m*; f'_c=28 *MPa*; f_y=420 *MPa*; q_a=250 *kN*/m^2; γ_{ppz}=24 *kN*/m^3; γ_{pps}=15 *kN*/m^3.

Where H is the depth of the footing, P_D is the dead load, P_L is the live load, M_{Dx} is the moment around the axis "*X-X*" of the dead load, M_{Lx} is the moment around the axis "*X-X*" of the live load, M_{Dy} is the moment around the axis "*Y-Y*" of the dead load, M_{Ly} is the moment around the axis "*Y-Y*" of the live load.

The loads and moments acting on soil are: P_1=1000 *kN*; M_{x1}=300 *kN-m*; M_{y1}=200 *kN-m*; P_2=500 *kN*; M_{x2}=150 *kN-m*; M_{y2}=200 *kN-m*.

The thickness of the footing is proposed, the first proposal is the minimum thickness of 25 cm in accordance with regulations of the ACI, and subsequently the thickness is revised to satisfy the following conditions: moments, bending shear, and punching shear. If such conditions are not satisfied, is proposed a greater thickness until it fulfills the three conditions mentioned. The thickness of the footing than fulfills the three conditions listed above is 90 cm (effective depth is 82 cm, and coating is 8 cm), the available load capacity of the soil "σ_{adm}" is 211.90 *kN*/m^2 (Gambhir 2008, González-Cuevas and Robles-Fernandez-Villegas 2005, McCormac and Brown 2013, Luévanos-Rojas *et al.* 2013, Luévanos-Rojas 2014a, b, 2015).

Substituting the values of "σ_{adm}=211.90 *kN*/m^2, L=6.00 m, P_1=1000 *kN*, M_{x1}=300 *kN-m*, M_{y1}=200 *kN-m*, P_2=500 *kN*, M_{x2}=150 *kN-m*, M_{y2}=200 *kN-m*, $b \geq$6.40 m, $b_1 \geq$1.50 m and $b_2 \geq$1.00 m" in Eqs. (29) to (42) of Part 1 and using the MAPLE-15 software for each case are obtained A_{tmin}=11.85 m^2, M_{xT}=259.27 *kN-m*, M_{yT}=400 *kN-m*, R=1500 *kN*, a=4.64 m, b=6.40 m, b_1=1.50 m, b_2=1.00 m, σ_1=211.09 *kN*/m^2, σ_2=67.71 *kN*/m^2, σ_3=202.31 *kN*/m^2, σ_4=145.76 *kN*/m^2, σ_5=114.66 *kN*/m^2, σ_6=58.11 *kN*/m^2, σ_7=114.43 *kN*/m^2, σ_8=83.32 *kN*/m^2.

Therefore the practical dimensions of the T-shaped combined footing supporting two square columns are a=4.70 m, b=6.40 m, b_1=1.50 m, b_2=1.00 m.

Substituting the values of a=4.70 m, b=6.40 m, b_1=1.50 m and b_2=1.00 m in the same MAPLE-15 software are found A_{tmin}=11.95 m^2, M_{xT}=243.20 *kN-m*, M_{yT}=400 *kN-m*, R=1500 *kN*, a=4.70 m, b=6.40 m, b_1=1.50 m, b_2=1.00 m, σ_1=208.06 *kN*/m^2, σ_2=67.62 *kN*/m^2, σ_3=199.10 *kN*/m^2, σ_4=143.82 *kN*/m^2, σ_5=113.94 *kN*/m^2, σ_6=58.66 *kN*/m^2, σ_7=114.56 *kN*/m^2, σ_8=84.66 *kN*/m^2.

Now, substituting the values of a=4.70 m, b=6.40 m, b_1=1.50 m and b_2=1.00 m in the Derive6 software are obtained: y_s=2.06 m, I_x=40.73 m^4, I_y=13.38 m^4.

The factored mechanical elements (P, M_x, M_y) acting on the footing are: P_{u1}=1.2P_{D1}+1.6P_{L1}=1360 *kN*;

M_{ux1}=1.2M_{Dx1}+1.6M_{Lx1}=416 *N-m*;

M_{uy1}=1.2M_{Dy1}+1.6M_{Ly1}=272 *kN-m*;

P_{u2}=1.2P_{D2}+1.6P_{L2}=680 *kN*;

M_{ux2}=1.2M_{Dx2}+1.6M_{Lx2}=208 *kN-m*;

M_{uy2}= 1.2M_{Dy2}+1.6M_{Ly2}=272 *kN-m*.

4. Results

Substituting the factored mechanical elements into Eqs. (4) and (5) is obtained M_{xT}=342.75 *kN-m*; M_{yT}=544 *kN-m*.

Now, substituting the dimensions of the footing, the dimensions of the columns, and the loads and factored moments that are applied on the columns to obtain the moments acting on critical sections of the T-shaped combined footing are shown: M_a=787.47 *kN-m*; M_b=89.35 *kN-m*; M_c=−617.71 *kN-m*; M_d=−1211.85 *kN-m*; M_e=−1229.60 *kN-m*; M_f=82.83 *kN-m*; M_g=0 *kN-m*.

The maximum moment "M_e" is presented in the interval "$y_s-(L+c_2/2) \leq y_2=y_m \leq y_s-b_1$", and y_m=0.11 m.

The effective depth to the maximum moment of the axes parallel to the axis "*Y-Y*" is: d=38.61 cm. The effective depth to the maximum moment of the axes parallel to the axis "*X-X*" is: d=43.42 cm. effective depth after performing different proposals is: d=82.00 cm, r=8.00 cm, t=90.00 cm.

Substituting the dimensions of the footing, the dimensions of the columns, and the loads and factored moments that are applied on the columns to obtain the bending shear forces acting on critical sections of the T-shaped combined footing are indicated: V_{fh}=−455.31 *kN*; V_{fi}=0 *kN*; V_{fj}=311.07 *kN*; V_{fk}=78.64 *kN*; V_{fl}=−510.01 *kN*; V_{fm}=0 *kN*. The bending shear force "V_{fj}" is localized in the interval "$y_s-b_1 \leq y_1=y_s-c_2-d$", and y_1=0.84 m. The bending shear resisted by the concrete to "V_{fh} and V_{fi}" is $\emptyset_v V_{cf}$=507.86 *kN*, and to "V_{fj}, V_{fk}, V_{fl} and V_{fm}" is $\emptyset_v V_{cf}$=626.99 *kN*. Therefore, the two conditions are accepted.

Table 1 Reinforcement steel of the new model

Reinforcement steel		Area cm^2
Reinforcement steel in direction the axis "Y"		
Steel at the top with a width of b_2	Main steel	41.52
	Minimum steel	27.33
	Steel proposed	45.54(9Ø1") Spacing 11.11 cm
Steel in the bottom with a width of b_2	Temperature steel	16.20
	Steel proposed	20.24(4Ø1") Spacing 25.00 cm
Steel at the top of the excess parts of the width b_2 $(a-b_2)$	Temperature steel	59.94
	Steel proposed	60.72(12Ø1") Spacing 30.83 cm
Steel in bottom of the excess parts of the width b_2 $(a-b_2)$	Temperature steel	59.94
	Steel proposed	60.72(12Ø1") Spacing 30.83 cm
Reinforcement steel in direction the axis "X"		
Steel at the top with a width of b	Temperature steel	103.68
	Steel proposed	106.26(21Ø1") Spacing 30.48 cm
Steel in the bottom under the column 1 with a width of w_1	Main steel	26.33
	Minimum steel	22.14
	Steel proposed	30.36(6Ø1") Spacing 13.50 cm
Steel in the bottom under the column 2 with a width of w_2	Main steel	2.89
	Minimum steel	22.14
	Steel proposed	25.30(5Ø1") Spacing 16.20 cm
Steel in bottom of the excess parts of the columns $(b-w_1-w_2)$	Temperature steel	77.44
	Steel proposed	80.96(16Ø1") Spacing 29.94 cm

Table 2 Development length

Concept	Steel at the top	Steel in the bottom
ψ_t	1.3	1.0
$\psi_e = \lambda$	1.0	1.0
l_d(cm)	178.02	110.85
l_a(cm)	161.00(Fails)	215.00(O.K.)

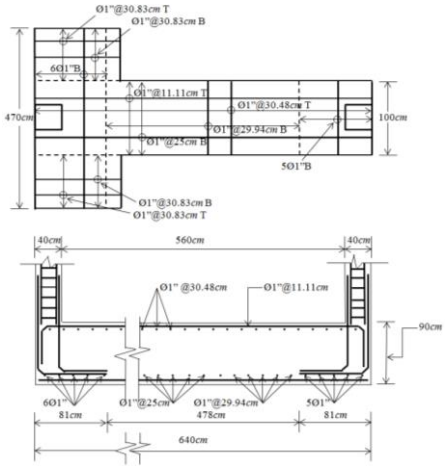

Fig. 5 Diagram for the T-shaped combined footing

Now, substituting the dimensions of the footing, the dimensions of the columns, and the loads and factored moments that are applied on the columns to obtain the punching shear forces acting on critical sections of the T-shaped combined footing are presented: V_{p1}=1177.52 *kN*; V_{p2}=704.52 *kN*. The punching shear resisted by the concrete to "V_{p1}" are $\emptyset_v V_{cp1}$=5241.96 *kN*, $\emptyset_v V_{cp1}$=7530.52 *kN*, $\emptyset_v V_{cp1}$=3456.56 *kN*, and to "V_{p2}" are $\emptyset_v V_{cp2}$=1880.97 *kN*, $\emptyset_v V_{cp2}$=8142.76 *kN*, $\emptyset_v V_{cp2}$=1217.10 *kN*. Therefore, the two conditions are accepted.

The reinforcement steel for the T-shaped combined footing is shown in Table 1.

The minimum development length for deformed bars appears in Table 2. The longitudinal reinforcement steel hook is provided in direction "*Y*" on top, i.e., where the column 1 is located. The transverse reinforcement steel hook is not needed in all the direction "*X*".

Fig. 5 shows the dimensions and the reinforcement steel of the T-shaped combined footing.

Effects that govern the design for the T-shaped combined footings are the moments, bending shear, and punching shear with regard to thickness of the concrete footings, and the reinforcement steel is governed by the moments.

A way to validate the new model is as follows: For the interval "$y_s-b \leq y_2 \leq y_s-(L+c_2/2)$" is substituted "$y_2=y_s-b$" into Eq. (50), the moment acting on footing is M_{x2}=0 *kN-m*. For the interval "$y_s-b \leq y_2 \leq y_s-(L+c_2/2)$" is substituted "$y_2=y_s-b$" into Eq. (47), the bending shear force acting on footing is V_{y2}=0 *kN*.

Therefore the new model in this paper is valid, because the equilibrium of the moments and the loads acting on the footing against the pressure exerted by the ground on the footing are verified.

5. Conclusions

The new model presented in this paper applies only for design of the T-shaped combined footings, the structural member assumes that should be rigid and the supporting soil layers elastic, which meet expression of the bidirectional bending, i.e., the variation of pressure is linear.

The presented new model at this paper is concluded the following:

1. The thicknesses for the new model of the T-shaped combined footings are governed by the bending shear, and the isolated footings are governed by the punching shear.

2. The new model is not limited with respect to the classic model that considers an axial load and a moment around the axis "X" (transverse axis) applied to each column, i.e., the resultant force from the applied loads is located on the axis "Y" (longitudinal axis), and its position must match with the geometric center of the footing.

3. The new model is adjusted to real conditions with respect to the classical model, because the new model taking into account the soil real pressure and the classical model considers the maximum pressure in all the contact surface, when the axial load and moments in two directions to each column are presented.

4. The new model for design of foundations subject to axial load and moments in two directions to each column considers one or two property lines restricted.

The new model presented in this paper for the structural design of the T-shaped combined footings subjected to an

axial load and moment in two directions in each column, also it can be applied to others cases: 1) The footings subjected to a concentric axial load in each column, 2) The footings subjected to an axial load and moment in one direction in each column.

The suggestions for future research, when is presented another type of soil, by example in totally cohesive soils (clay soils) and totally granular soils (sandy soils), the pressure diagram is not linear and should be treated differently (see Fig. 1).

Acknowledgments

The research described in this paper was financially supported by the Institute of Multidisciplinary Researches of the Faculty of Accounting and Administration of the Autonomous University of Coahuila. The authors also gratefully acknowledge the helpful comments and suggestions of the reviewers, which have improved the presentation.

References

ACI 318S-13 (American Concrete Institute) (2013), *Building Code Requirements for Structural Concrete and Commentary*, ACI Committee 318.

Agrawal, R. and Hora, M.S. (2012), "Nonlinear interaction behaviour of infilled frame-isolated footings-soil system subjected to seismic loading", *Struct. Eng. Mech.*, **44**(1), 85-107.

Bowles, J.E. (2001), *Foundation Analysis and Design*, McGraw-Hill, New York, U.S.A.

Calabera-Ruiz, J. (2000), *Calculo de Estructuras de Cimentación*, Intemac Ediciones, Mexico.

Chen, W.R., Chen, C.S. and Yu, S.Y. (2011), "Nonlinear vibration of hybrid composite plates on elastic foundations", *Struct. Eng. Mech.*, **37**(4), 367-383.

Cure, E., Sadoglu, E., Turker, E. and Uzuner, B.A. (2014), "Decrease trends of ultimate loads of eccentrically loaded model strip footings close to a slope", *Geomech. Eng.*, **6**(5), 469-485.

Das, B.M., Sordo-Zabay, E. and Arrioja-Juarez, R. (2006), *Principios de Ingeniería de Cimentaciones*, Cengage Learning Latin America, Mexico.

Dixit, M.S. and Patil, K.A. (2013), "Experimental estimate of Nγ values and corresponding settlements for square footings on finite layer of sand", *Geomech. Eng.*, **5**(4), 363-377.

Erzín, Y. and Gul, T.O. (2013), "The use of neural networks for the prediction of the settlement of pad footings on cohesionless soils based on standard penetration test", *Geomech. Eng.*, **5**(6), 541-564.

Gambhir, M.L. (2008), *Fundamentals of Reinforced Concrete Design*, Prentice-Hall of India Private Limited.

Gere, J.M. and Goodno, B.J. (2009), *Mecánica de Materiales*, Cengage Learning, Mexico.

González-Cuevas, O.M. and Robles-Fernández-Villegas, F. (2005), *Aspectos fundamentales del concreto reforzado*, Limusa, Mexico.

Guler, K. and Celep, Z. (2005), "Response of a rectangular plate-column system on a tensionless winkler foundation subjected to static and dynamic loads", *Struct. Eng. Mech.*, **21**(6), 699-712.

Kurian, N.P. (2005), *Design of Foundation Systems*, Alpha Science Int'l Ltd., India.

Luévanos-Rojas, A. (2014a), "Design of isolated footings of circular form using a new model", *Struct. Eng. Mech.*, **52**(4), 767-786.

Luévanos-Rojas, A. (2014b), "Design of boundary combined footings of rectangular shape using a new model", *Dyna-Colombia*, **81**(188), 199-208.

Luévanos-Rojas, A. (2015), "Design of boundary combined footings of trapezoidal form using a new model", *Struct. Eng. Mech.*, **56**(5), 745-765.

Luévanos-Rojas, A. (2016a), "A comparative study for the design of rectangular and circular isolated footings using new models", *Dyna-Colombia*, **83**(196), 149-158.

Luévanos-Rojas, A. (2016b), "Un nuevo modelo para diseño de zapatas combinadas rectangulares de lindero con dos lados opuestos restringidos", *Revista ALCONPAT*, **6**(2), 172-187.

Luévanos-Rojas, A., Faudoa-Herrera, J.G., Andrade-Vallejo, R.A. and Cano-Alvarez M.A. (2013), "Design of isolated footings of rectangular form using a new model", *J. Innov. Comput. Inform. Control*, **9**(10), 4001-4022.

Maheshwari, P. and Khatri, S. (2012), "Influence of inclusion of geosynthetic layer on response of combined footings on stone column reinforced earth beds", *Geomech. Eng.*, **4**(4), 263-279.

McCormac, J.C. and Brown, R.H. (2013), *Design of Reinforced Concrete*, John Wiley & Sons, New York.

Mohamed, F.M.O., Vanapalli, S.K. and Saatcioglu, M. (2013), "Generalized schmertmann equation for settlement estimation of shallow footings in saturated and unsaturated sands", *Geomech. Eng.*, **5**(4), 363-377.

Orbanich, C.J. and Ortega, N.F. (2013), "Analysis of elastic foundation plates with internal and perimetric stiffening beams on elastic foundations by using finite differences method", *Struct. Eng. Mech.*, **45**(2), 169-182.

Orbanich, C.J., Dominguez, P.N. and Ortega, N.F. (2012), "Strenghtening and repair of concrete foundation beams whit fiber composite materials", *MaterStruct.*, **45**, 1693-1704.

Punmia, B.C., Kumar Jain, A. and Kumar Jain, A. (2007), *Limit State Design of Reinforced Concrete*, Laxmi Publications (P) Limited, New Delhi, India.

Rad, A.B. (2012), "Static response of 2-D functionally graded circular plate with gradient thickness and elastic foundations to compound loads", *Struct. Eng. Mech.*, **44**(2), 139-161.

Shahin, M.A. and Cheung, E.M. (2011), "Stochastic design charts for bearing capacity of strip footings", *Geomech. Eng.*, **3**(2), 153-167.

Smith-Pardo, J.P. (2011), "Performance-based framework for soil-structure systems using simplified rocking foundation models", *Struct. Eng. Mech.*, **40**(6), 763-782.

Tomlinson, M.J. (2008), *Cimentaciones, Diseño y Construcción*, Trillas, Mexico.

Uncuoğlu, E. (2015), "The bearing capacity of square footings on a sand layer overlying clay", *Geomech. Eng.*, **9**(3), 287-311.

Varghese, P.C. (2009), *Design of Reinforced Concrete Foundations*, PHI Learning Pvt. Ltd., New Delhi, India.

Zhang, L., Zhao, M.H., Xiao, Y. and Ma, B.H. (2011), "Nonlinear analysis of finite beam resting on winkler with consideration of beam-soil interface resistance effect", *Struct. Eng. Mech.*, **38**(5), 573-592.

CC